RSC Advances

ROYAL SOCIETY OF CHEMISTRY

www.rsc.org/advances

Development of ternary iron vanadium oxide semiconductors for their applications in Photoelectrochemical Water Oxidation

Harahari Mandal[a], Sanjib Shyamal[a], Paramita Hajra[a], Aparajita Bera[a], Debasis Sariket[a], Sukumar Kundu[b], Chinmoy Bhattacharya[a*]

[a] *Department of Chemistry,* [b] *Department of Metallurgy & Materials Engineering*

Indian Institute of Engineering Science & Technology,(IIEST), Shibpur,

Howrah – 711103, West Bengal, INDIA

Email: cbhattacharya.besus@gmail.com

Abstract

In the present work we report synthesis of Fe-V-Oxides by drop casting metal precursor solutions of different proportions onto indium tin oxide (ITO) coated glass followed by annealing in air at 500°C for 3 h. UV-vis spectroscopy of the Fe-V-oxides indicates absorption due to 'direct' and 'indirect' band gap whereas Fe-oxide shows direct band gap nature. Scanning electron microscopy-energy dispersive X-ray (SEM-EDX) and X-ray diffraction (XRD) study reveal different surface morphology with variable crystalline phases for the Fe_2O_3, $FeVO_4$, FeV_2O_4 and Fe_2VO_4 semiconductors. The photoelectrochemical (PEC) water oxidation reaction over the different materials revealed that the FeV_2O_4 semiconductor exhibit maximum photocurrent of 0.18 mA cm^{-2} at an applied bias of +1.0 V (vs Ag/AgCl) under illumination of 100 mW cm^{-2} compared to other Fe_2O_3, $FeVO_4$ and Fe_2VO_4 semiconductors. Electrochemical impedance spectroscopic (Mott-Schottky) analysis confirms n-type semiconductivity for all the materials with highest donor density, of the order of $2.7x10^{20}$ cm^{-3}, for FeV_2O_4 thin film and PL spectra are useful for

measuring the separation efficiency of the photo-generated charge carriers. Chronoamperometric studies under constant illumination of the best semiconductor (FeV_2O_4) indicates significant stability to the material and photoelectrochemical action spectra measures 22% of the incident photon to current conversion efficiency (IPCE) and 60% absorbed photon to current conversion efficiency (APCE).

Keywords: Drop-cast method; Semiconductor photoelectrochemistry; Electrochemical action spectra; Incident photon to current conversion efficiency (IPCE); Electrochemical impedance spectroscopy,

1. Introduction

We prepare a stable and low cost Fe-based semiconductor (SC) that can absorb a large portion of the solar photons while having a minimum band gap energy. Most of the stable semiconductors absorb almost exclusively in the UV region of the solar spectrum[1,2]. Iron (III) oxide (Fe_2O_3) with a band gap of ~ 2.2 eV can absorb most of the visible light (300 to 560 nm), of the solar radiation, which comprises 38% of the photons of sunlight at air mass (AM) 1.5 spectra. Even though the band gap of Fe_2O_3 is suitable to allow absorption of a significant photon of sunlight, its photoresponse is quite low, mainly due to low electrical conductivity and high recombination rate of photogenerated electron-hole pairs[3,4]. To minimize these limitations, n-type iron (III) oxide SC has been modified with incorporating different proportions of vanadium[5,6] into its matrix with an aim to enhance the photoelectrochemical water oxidation[1,7,8] behavior. The goal of this work is to synthesize Fe-V-Oxide films of different composition by using a drop cast method and determine their efficacy toward a photoelectrochemical water splitting process [9,10]. As solar hydrogen is a sustainable and environment-friendly energy carrier, it is considered to replace fossil fuels in the near future. It can be generated by splitting of water under solar light

illumination[11,12,13]. The search for stable, efficient and affordable PEC electrode materials[14,15,16,17] (photoanodes and photocathodes), is an on-going quest. Hematite, α-Fe_2O_3, remains an intriguing choice for the oxygen-evolving photoanode material because of its environmentally benign chemical stability[18,19], its low price and its visible absorptivity character[20]. Recent theoretical and computational works support that hematite remains a promising parent material for artificial photosynthesis[21] undergoing water oxidation and CO_2 reduction reaction. Its bulk and surface electronic structure has been under scrutiny for many decades and is considered for improvement of efficiency[18].

Herein, we report synthesis of visible light responsive V incorporated Fe-Oxide compound SC. These composite demonstrate photocatalytic activity for oxygen evolution from water, under UV-vis illumination. Fe-V-Oxide[22] compound theoretical calculations which predicted a decrease of ~2.8 eV in the band gap with the Fermi level in the middle of the valence band maximum and conduction band minimum.

This work further demonstrates that improvement of the visible-light photocatalytic behavior for both water splitting and solar-energy conversion.

2. Experimental Section

2.1. Reagents. Iron (III) nitrate nonahydrate [$Fe(NO_3)_3,9H_2O$], and ammonium metavanadate (NH_4VO_3) were purchased from Sigma-Aldrich, NaH_2PO_4, Na_2HPO_4, Na_2SO_4, Na_2SO_3, ethylene glycol (EG) was purchased from Merck (AR quality) and used as received condition. All metal precursor solutions were prepared in ethylene glycol (EG) at a 0.1 M concentration. Milli-Q grade water was used in all the experiments to prepare the solutions. 2.0 × 1.5 cm^2 ITO-coated glass slides (Xinyan

technology Ltd, Hong Kong) were thoroughly cleaned by sonication in successive solutions of soap water followed by in ethanol and finally rinsed with Milli-Q water.

2.2. Preparation of thin film electrodes through drop casting technique.

Appropriate solutions with Fe:V (v/v) of the ratios of 1:0,1:1,1:2 and 2:1 were taken in EG in separate glass vials, and the mixtures were kept in ultrasonication bath for ~1hour. 500 µl of each of the mixtures was dropped cast onto the cleaned ITO substrate to prepare the semiconductor films. The thin films were annealed in air at 500°C with a ramping rate of heating of 1°C min^{-1} followed by soaking 3 h to obtain the uniform, well-adhered thin films. The thickness (t) of the films were measure gravimetrically using the relation

$$t = m / \rho A \qquad \text{----------(1)}$$

where, m and A stand for mass and area of the deposited film and ρ the density of the Fe_2O_3 and Fe-V-Oxide films, the thickness are found to be 260 nm for Fe_2O_3, 396 nm for $FeVO_4$, 480 for FeV_2O_4 nm and 481 nm for Fe_2VO_4 .

2.3. Optical Characterization. Absorption spectra of the prepared thin films was measured using V-630 UV-vis Spectrophotometer (Jasco, Japan) within the wavelength range of 350-700 nm, and the band gap energy was calculated from the absorption edge on the wavelength scale.

2.4. Photoluminescence study.

The photoluminescence spectra of the Fe_2O_3 and Fe-V-Oxide thin film semiconductors were obtained using a PerkinElmer LS 55 Fluorescence Spectrometer at an excitonic wavelength of 360 nm.

2.5. Surface characterization through SEM, XRD and EDX measurements.

The surface morphology and quality of the film on ITO coated glass substrate was determined through scanning electron microscopic (SEM) analysis using HITACHI S3400N Instrument. The elemental composition was further determined by energy dispersive X-ray (EDX) spectroscopic analyses of the samples[23] using 7021-H HORIBA EMAX Instrument installed with the SEM. The crystalline behavior of the prepared semiconductor was evaluated through powder X-ray diffraction (XRD) technique recorded with a Rigaku miniflex II, operated with a Cu Kα target (λ = 1.54Å) within the 2θ range of 20 to 80° at a fixed scan rate of 2° min^{-1}.

2.6. Photoelectrochemical measurement.

Photocurrent density measurements were performed by linear sweep voltammetry (LSV) using the CHI-650 potentiostat (CH Instrument, Austin, TX) in a standard three-electrode configuration cell (0.27 cm^2 geometric area exposed, using one O-ring of the same inner area) with a scan rate of 10 mVs^{-1}. The as prepared Fe-V-Oxide films served as the photoanode, Pt wire as the counter electrode and Ag/AgCl as the reference electrode and all the potential reported herein are with respect to this reference electrode. Measurements were carried out either in 0.1 M Na_2SO_4 with 0.1 M Na_2SO_3 as a sacrificial electron donor within the potential range of -0.1 to 0.6

V or in the presence of 0.1 M Na_2SO_4 in 0.1 M phosphate buffer solution (PBS) for water oxidation within the range of 0.0 to 1.2 V. A 100 mW cm^{-2} illumination was maintained through a 300 W Xe arc lamp (Excelitas USA) was used as a light source for this study. Visible-light responsiveness of the semiconductors towards photo-oxidation of water was carried out by holding a UV cut-off filter (λ > 420 nm) in front of the Xe lamp. The PEC measurements were carried out by irradiating the prepared electrodes through the electrolyte /electrode interface.

2.7. Chronoamperometric measurement.

Stability of the thin-film semiconductor electrode undergoing solar driven water oxidation reaction was evaluated through continuous photocurrent measurements for 30 min in 0.1 M Na_2SO_4-PBS when the electrode was held at a constant potential of 1.0 V under 100 mW cm^{-2} illumination. A monochromator (Oriel) was used in combination with a power meter and a silicon detector (Newport) to measure the photocurrent spectrum. From the electrochemical action spectra, incident photon to current conversion efficiency (IPCE) and absorbed photon to current conversion efficiency (APCE) was calculated.

2.8. Electrochemical impedance spectroscopic analysis of the semiconductor-electrolyte interface.

Electrochemical impedance spectroscopic (EIS) measurements were obtained using the similar experiment setup as stated above, at a constant applied potential of 1.0 V within the frequency range of 20 mHz to 100 kHz with oscillation amplitude of 10 mV. Experiments were carried out in dark and illuminated (UV-vis and only visible)

condition. Mott-Schottky experiment was carried out in 0.1 M Na_2SO_4 in 0.1 M phosphate buffer solution (PBS) using different frequencies of 200, 500 and 1000 Hz at an applied potential ranging from -0.4 to 0.8 V maintaining an ac amplitude of 10 mV at each of the potentials.

3. Results and discussion

3.1. Physicochemical characterization.

Thin film Fe-V-Oxide semiconductors were synthesized by drop-casting using Fe^{3+} and V^{5+} as the precursor in EG solution. The color of the individual precursor solution and the corresponding semiconductor thin films developed on ITO coated glass substrates, are presented in Fig. S1 (a and b), respectively (supporting information).

It has been observed that with gradual addition of V to pure Fe_2O_3 matrix, the color of the solution as well as that of the films changes from deep reddish to light yellow. Fig. 1a, represents the UV-visible absorption spectra of the different thin film semiconductors, and Fig. 1b (inset) represents the Tauc plot for calculation of band gap energy as well as to determine the nature of the band-to-band transition pattern. Tauc plot indicates absorption characteristics due to the distinct 'direct' band gap at ~1.9 eV and 'indirect' band gap at 2.6-2.7eV for the Fe-V-Oxides imparting yellow color to the film, whereas presence of a pure 'direct' band gap ~2.0 eV for the Fe-oxide make the film reddish in color. The thickness of the different materials is found to vary as 260 nm for Fe_2O_3, 396 nm for $FeVO_4$, 480 for FeV_2O_4 nm and 481 nm for Fe_2VO_4.

Photoluminescence (PL) emission spectra characterizes the recombination of free carriers, thus highlights the separation efficiency of the photo-generated charge carriers in a semiconductor[24,25,26]. The higher the PL intensity, the greater is the probability of charge carrier recombination[27]. A comparison of the PL spectra

(excited at 360 nm) of Fe_2O_3 and the Fe-V-Oxide compounds at room temperature has been presented in Fig. 2. The PL spectrum indicates a strong peak at ~480 nm region corresponding to high-level transition in Fe-V-Oxide. Among the different samples, FeV_2O_4 with lowest intensity at that particular region demonstrates that the recombination process can be effectively controlled inside the matrix. Therefore, FeV_2O_4 is much effective for separating the photo-generated charge carriers, which in turns triggers the charge transfer process at a faster rate than the other semiconductor thin films.

SEM analysis reveals the surface morphology of the thin-film semiconductors. Fig. 3 (a-d), represent the SEM images for the Fe-V-oxide compounds grown over the ITO coated glass substrates. For the pure iron oxide material, as presented in Fig. 3a, the surfaces are found to be covered with agglomerated particles. With addition of 33% V to the matrix, surface morphology (Fig. 3b) changes significantly with appearance of 'cubic' particle of approximate size of 250-300 nm. On addition of 50% V, the morphology changes to '3D triclinic' form of average length 800-1000 nm along with presence of some cubic forms (Fig. 3c). With further addition of to V (70 % V), the surface was found to be covered with small particles along with 'cylindrical' shaped particles with an average diameter in the order of 300-400 nm (Fig. 3d).

The EDX analysis of the different semiconductor thin films measures the individual elemental compositions (atomic percentage %) of the constituents. Fig 4(a-d) represents the elemental mapping of Fe-V-Oxide compounds whereas Fig. 4e (bar plot) indicates the relative proportions of the individual elements in the semiconductor matrix. The composition analysis well corresponds to the prepared semiconductors developed through drop-casting techniques.

Crystalline natures of the as-prepared samples were examined by XRD technique. Fig. 5, represents the XRD pattern for pure Fe-oxide and is identified as α-Fe_2O_3 (hematite) compounds with 'Rhombohedral' geometry (JCPDS file 79-1741). Addition of different levels of vanadium to the Fe-oxide leads to the change in the crystallinity of the semiconductors to a significant extent. 33% V added material has been identified as Fe_2VO_4 using JCPDS file 75-1519 with 'cubic' structure, whereas 50% V added film marked as $FeVO_4$ with JCPDS file 71-1592 showing preferential 'triclinic' nature. The compound containing 70% of V shows 'Cubic' structure, as marked with JCPDS file 75-0317 and have been identified as FeV_2O_4. Different peaks in the XRD pattern for all the materials have been indexed with the corresponding (hkl) values comparing with the standard JCPDS data file.

The crystallize size D (in Å), of the strongest peaks for each of the XRD patterns were analyzed using the Scherrer formula.

$$D = (0.9\lambda)/(\beta \cos \theta) \quad \text{----------} \quad (2)$$

where 'λ' is wavelength of X-ray (1.54 Å), 'β' is FWHM (full width at half maxima, in degree), 'θ' is the diffraction angle (in degree). The value of d, the interplanar spacing between the atoms, is calculated using the Bragg's Law.

$$n\lambda = 2d \sin\theta \quad \text{----------} \quad (3)$$

The average sizes of the crystallites corresponding to the strongest peaks for each of the Fe_2O_3 (104), $FeVO_4$ (311), FeV_2O_4 (311) and Fe_2VO_4 (112) were calculated as 21 nm, 23 nm, 23 nm and 26 nm respectively.

3.2. Photocurrent Measurements.

Three-electrode cell setup with an area of 0.27 cm^2 exposed SC surface as working electrode (WE) was used to study the photoelectrochemical (PEC) behavior of these

compounds under periodic chopped UV-visible illumination of 100 mW cm^{-2}. Fig. 6a, represents the linear sweep voltammogram for photo oxidation of the sacrificial reagent (SO_3^{2-}) over different SC surface at a scan rate of 10 mV s^{-1}, within the potential range of -0.1 to 0.6 V. Fig. 6b; inset represents the bar plot, i.e variation of photocurrent as measured from LSV (Fig. 6a) at a potential of 0.5V, for these compounds which indicate that FeV_2O_4 exhibits the highest photocurrent than others. Water oxidation behaviors of these SC materials were evaluated through LSV plot Fig. 7a in 0.1 M SO_4^{2-} and 0.1 M phosphate buffer solution (pH 7) within the potential range of 0.0 to 1.2 V and the variation of photocurrent for the different materials at 1.2V has been presented in the bar plot (Fig. 7b, inset). Similar to the observed for sacrificial oxidation, in this case also the highest photocurrent is observed for FeV_2O_4 compound SC, which attains a value of 0.18 mA cm^{-2} at 1.2 V. Visible-light responsiveness of the semiconductors towards water oxidation was carried out by holding a UV cut-off filter (λ > 420 nm) in front of the Xe lamp. Fig. S2 (supporting information), represents the comparative behavior of FeV_2O_4 film undergoing the water oxidation process where the material retains ~30% photo-performance when exposed to periodic VU-vis and visible illuminations.

Stabilities of the semiconductor electrodes were verified through chronoamperometry by holding a fixed potential of 1.0 V vs Ag/AgCl for the photoelectrochemical oxidation of water under constant illumination of 100 mW cm^{-2}. Fig. 8, represents the chronoampherometric (current-time) diagram of all semiconductors where FeV_2O_4 indicates fairly stable water oxidation behavior for at least 30 minutes. Gradual decrease in photocurrent for much longer exposure may be ascertained due to steady recombination of the photo-generated electrons and holes within the bulk of the SC matrix.

Electrochemical action spectra was obtained under periodic chopped monochromatic illumination. Fig. 9 represents the photoelectrochremical action spectrum for all of the semiconductors in 0.1 M Na_2SO_4 in presence of PBS measured at 1.0 V with gradually change in monochromatic light wavelength from 250 to 620 nm. The corresponding photocurrent at each wavelength was calculated from the action spectra, and has been presented in Fig. S3 (supporting information). The onsets of photocurrent for the different semiconductors (Fe_2O_3, Fe_2VO_4, $FeVO_4$ and FeV_2O_4) are found to be 560, 580, 600 and 610 nm corresponding to the 'true' or photoelectrochemical band gap of the materials as 2.21, 2.13, 2.06 and 2.03 eV, respectively.

The IPCE measurement showed a clear wavelength dependence of the photocurrent generation. The incident photon to current conversion efficiency (IPCE) measurement was performed with monochromatic irradiation employing a 300 W Xe arc lamp attached with an optical power meter (Oriel) was used. The IPCE (%) was calculated from the equation,

$$IPCE(\%)=(1240/\lambda)\times(I_{Ph}/P_{in})\times 100 \quad \text{----------(4)}$$

where, λ is the wavelength of the incident light in nm, I_{Ph} is the photocurrent in mA cm^{-2} and P_{in} is the power of the incident beam in 100 mW cm^{-2} of monochromatic light, respectively. The applied potential was monitored against an Ag/AgCl reference, and the absorbed photon to current conversion efficiency (APCE) was further calculated by considering the absorbance (A_λ) of the material at that particular wavelength using the following equation.

$$APCE(\%) = (IPCE/1-10^{-A_\lambda})\times 100 \quad \text{----------(5)}$$

Fig. 10a and b, represent variation of %IPCE and %APCE, respectively, for the different materials, and it has been observed that FeV_2O_4 semiconductor exhibits

highest photoconversion efficiency of IPCE as 22%, and corresponding APCE as 60%, compared to other Fe-V-oxides.

3.3. Capacitance Mesurement. Mott-Schottky (M-S) plot, the linear variation of $1/C^2$ (space charge capacitance in F cm^{-2}) with respect to the applied potential can be expressed using the relation shown in equation 6.

$$\frac{1}{C^2} = \frac{2}{\varepsilon_s \varepsilon_0 A^2 e N_D} \left(E - E_{fb} - \frac{k_B T}{e}\right) \quad \text{..... (6)}$$

Where ε_s is the dielectric constant of the semiconductor, ε_0 is the permittivity of free space, e is the electronic charge in C, N_D is the donor density (per cc), E is the applied potential in V, E_{fb} is the flat band potential in V, k_B is the Boltzmann's constant and T is the temperature in absolute scale. The flat band potential of the semiconductor – electrolyte interface can be obtained from the intercept on the potential axis whereas the slope of the straight line is inversely related to the carrier concentration, N_D ($Slope = \frac{2}{\varepsilon_s \varepsilon_0 A^2 e N_D}$). The positive slope of the M-S plots, as shown in Fig. 11, confirms the n-type semiconductivity for all of the material and the estimated flat band potentials for Fe_2O_3, Fe_2VO_4, $FeVO_4$ and FeV_2O_4 are obtained from the intercept of the tangent line of the M-S plots on potential axis as -0.15,c -0.10, 0.08 and 0.07V, respectively. Positive shifting of the flat band potentials with gradual addition of %V to the matrix may favor the overall charge transfer kinetics across the semiconductor-electrolyte interface. The donor densities of the Fe-V-Oxide compound semiconductors of different compositions were calculated from the slope of the respective M-S plot using the respective dielectric constants (ε_s) of the materials as Fe_2O_3: 14.2[28]; $FeVO_4$: 14.78[29] and FeV_2O_4: 7.0[30]; and considering that for Fe_2VO_4 as same for the $FeVO_4$ due to unavailability of its data. Orders of the

slopes of the M-S plots are found to be quite similar to values reported for similar Fe-oxide based semiconductor materials[18]. Relatively higher carrier concentration of FeV_2O_4 matrix ($2.7x10^{20}$ cm^{-3}) may lead to reduce in ohmic resistivity of the film and thereby improving the photoelectrochemical water oxidation performance, as observed in LSV Plots. M-S plots, measured at 200, 500 and 1000Hz using FeV_2O_4 have been presented in Fig. S4 (supporting information) which indicates frequency independent behavior through the analysis.

The energy band diagram for the different Fe-V-Oxide compounds has been presented in Fig. 12 showing the conduction band (CB) position, near to their flat band positions and the corresponding valence band (VB), considering their individual band gap energies. The redox potential of the photo-generated holes (+1.8-1.9 V vs. Ag/AgCl) is high enough to drive the water oxidation reaction ($H_2O \rightarrow O_2$, E^0 +0.59V vs. Ag/AgCl at pH 7), and the material exhibits excellent photoelectrochemical oxidation behavior.

3.4. Impedance Measurements.

The frequency dispersive impedance data were collected for all the materials and the typical Nyquist plot showing the variation of real and imaginary part of the impedance, under UV-vis illumination, has been presented in Fig. 13a. The Nyquist plots were analyzed based on the equivalent circuit model (Fig. 13b) which includes a solution resistance (R_s), charge-transfer resistance (R_{ct}) and the double-layer capacitance (C_{ct}) associated to the charge transfer process. In the present case, the charge-transfer resistance (R_{ct}) values of the different materials are found to vary as Fe_2O_3, $FeVO_4$, Fe_2VO_4 and FeV_2O_4 are 102, 45, 25 and 23 kohm, respectively. In fact, a material with low R_{ct} and high C_{ct} value is generally considered suitable for

use in PEC cell as photo-electrode due to their efficiency in transfer of charge carriers across the semiconductor–electrolyte interface and better semiconductivity of the film matrix.

In the present case, minimum value of R_{ct} and relative higher C_{ct} for the FeV_2O_4 compound semiconductor supports superior photoelectrochemical oxidation behavior of the material. Fig. S5 (supporting information) represents the impedance data of FeV_2O_4 in dark, visible and UV-visible conditions indicating the facile charge transfer reaction in presence of UV-vis light.

4. Conclusion.

Iron vanadium oxide semiconductor thin films of different compositions have been prepared on ITO coated glass substrate at 500^{o}C temperature. EDX analysis further confirms the presence of iron, vanadium and oxygen in the films almost to the same order, as prepared through drop-casting technique. The semiconductor electrodes are found to remain almost stable, at least for half an hour in aqueous electrolytes at pH 7 under light illumination of 100 mW cm^{-2}. Fe-V-oxides show a direct band gap at ~1.9 eV and indirect gap at ~2.6-2.7eV attributed to significant visible-light responsiveness of the materials for water oxidation reaction. FeV_2O_4 semiconductor with a distinct surface morphology exhibits the highest photocurrent due to its high carrier concentration, low charge transfer resistance and higher double layer capacitance. Photoconversion efficiency of 22% IPCE and 60% APCE has been recorded with FeV_2O_4 semiconductor material towards O_2 evolution reaction from water.

Acknowledgement

Financial support through the sponsored project grant of the Govt. of India from SERB-DST (Sanction Order No.SB/S1/PC-042/2013, dt. 28-05-2014), & BRNS-DAE (Sanction Order No.2013/37C/61/BRNS, dt. 03-12-2013) and from DST, Govt. of West Bengal, (Sanction order no. 902(Sanc.)/ST/P/S & T/4G – 1/2013, dt. 08/01/2015) to the Department of Chemistry, IIEST, Shibpur are gratefully acknowledged. Instrumental support from the MHRD, UGC-SAP to the Department of Chemistry, IIEST, Shibpur is also gratefully acknowledged.

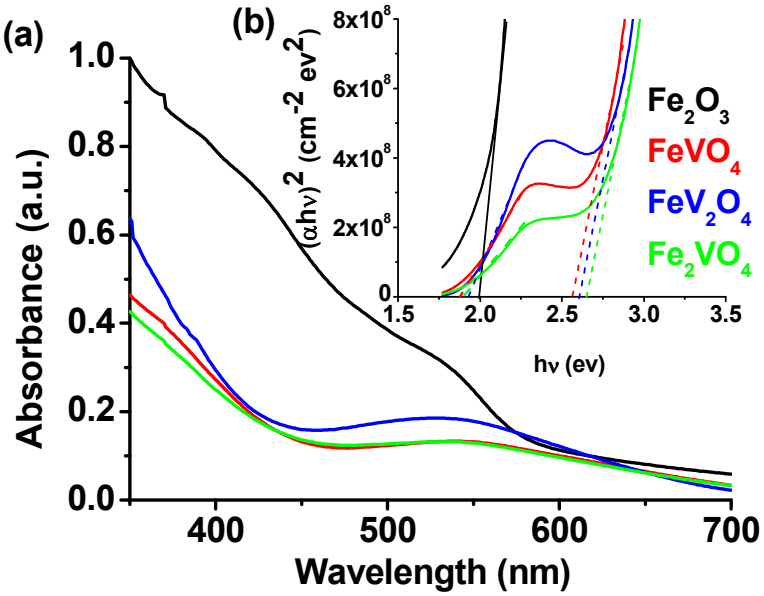

Fig. 1 (a) Absorption spectra for determination of band gap energy of Fe-V-Oxide compound thin film semiconductor prepared with 500 µl solution on the glass substrate. **(b) Inset:** Tauc plot of same film semiconductors showing 'direct' and 'indirect' gaps.

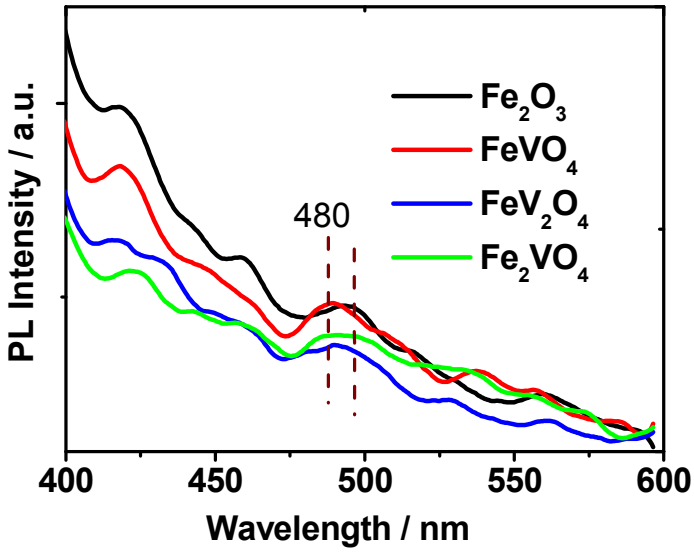

Fig. 2 PL spectra of the Fe-V-Oxide semiconductors excited at 360 nm.

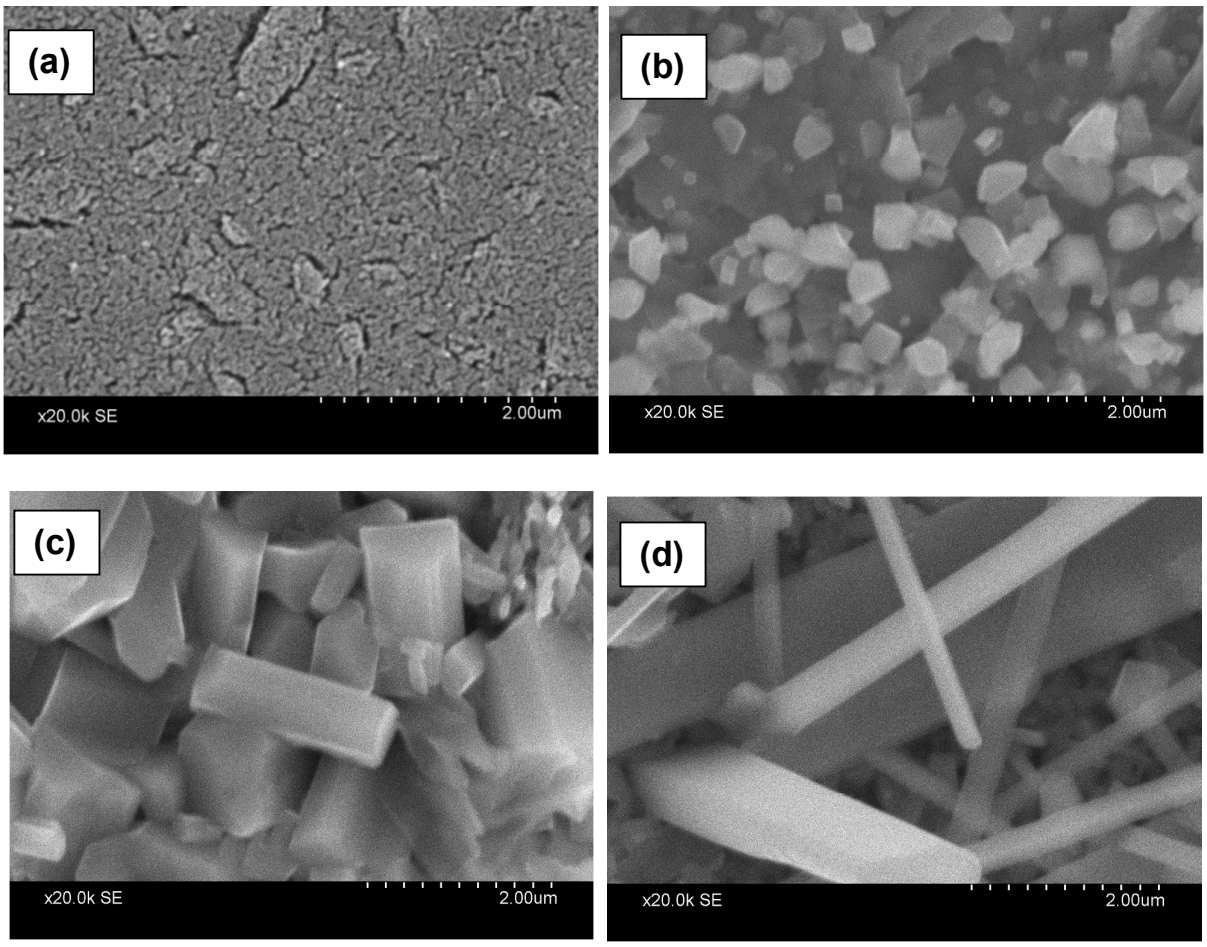

Fig. 3(a-d) SEM images of (a) Fe_2O_3; (b) Fe_2VO_4; (c) $FeVO_4$ and (d) FeV_2O_4 films on ITO coated glass substrates annealed at 500°C for 3h.

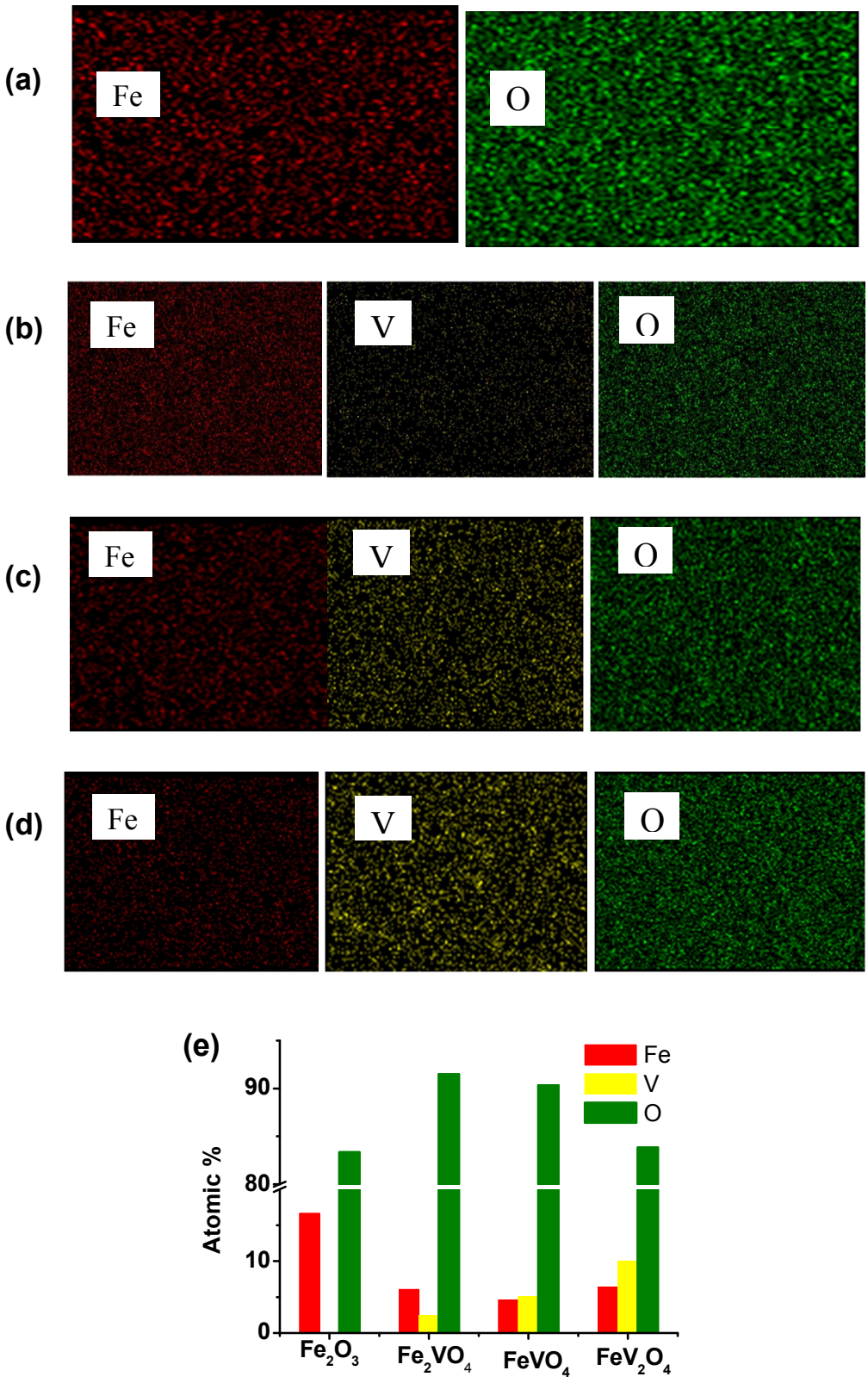

Fig. 4 (a-e) EDX elemental mapping of (a) Fe_2O_3, (b) Fe_2VO_4, (c) $FeVO_4$, (d) FeV_2O_4 and (e) atomic percentage (%) of Fe (red), V (yellow) and O (green).

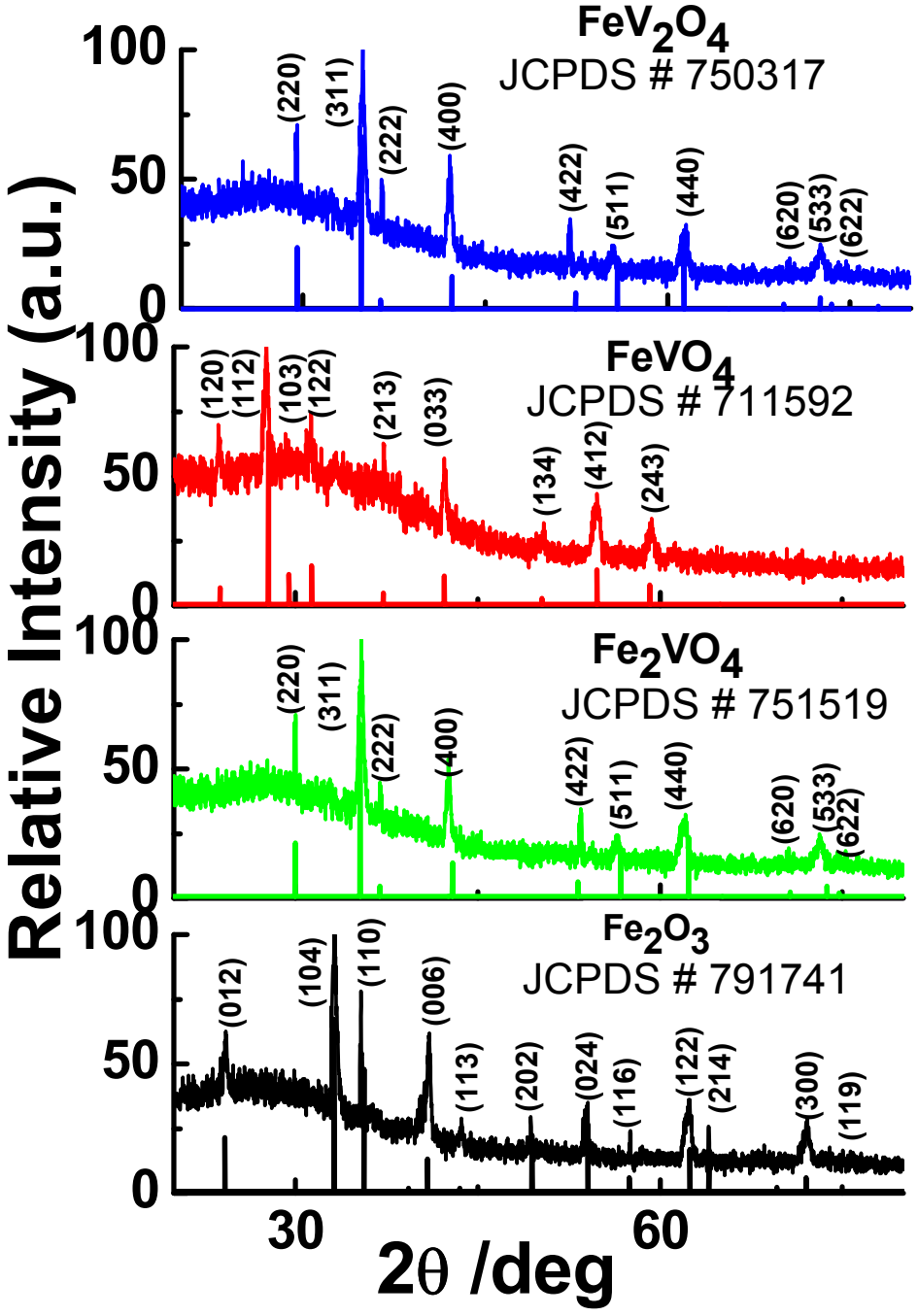

Fig. 5 XRD pattern of Fe-V-Oxide compound semiconductor films annealed at 500°C for 3 h on ITO conducting glass.

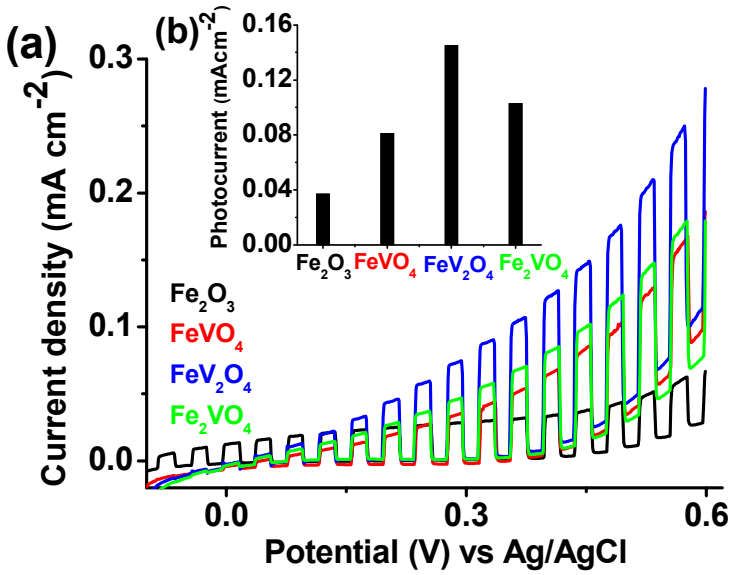

Fig. 6 (a) Linear sweep voltammetry of Fe-V-Oxide semiconductor electrodes in 0.1 M SO_3^{2-}- SO_4^{2-} solution in presence of UV-vis light (intensity: 100mW / cm^2). (b **inset),** Variation of photocurrent (I_{ph}) at 0.5 V for the different materials.

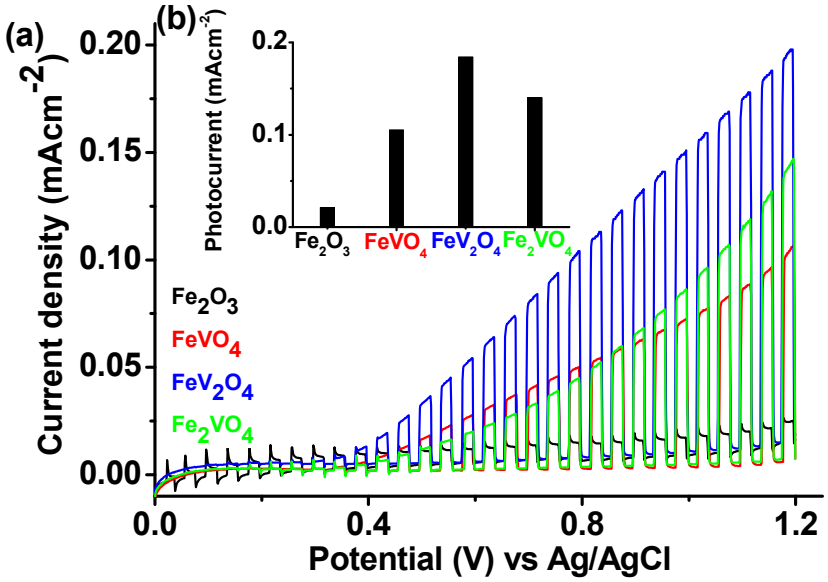

Fig. 7 (a) Linear sweep voltammetry of Fe-V-Oxide semiconductor electrodes in 0.1M SO_4^{2-}-phosphate buffer solution (for water oxidation) in presence of UV-Vis light (intensity: 100 mW /cm^2). (b **inset),** Variation of photocurrent (I_{ph}) at 1.2 V for the different materials.

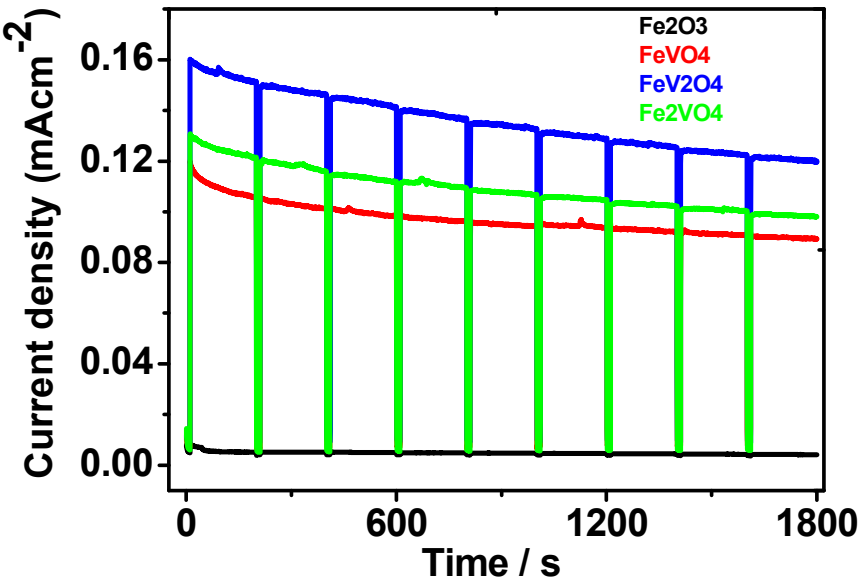

Fig. 8 Current-time response (chronoamperometry) curve of the Fe-V-Oxide semiconductors at an applied potential of 1.0 V in 0.1 M Na_2SO_4 with a 0.1 M phosphate buffer solution (pH 7) under UV−vis light irradiation.

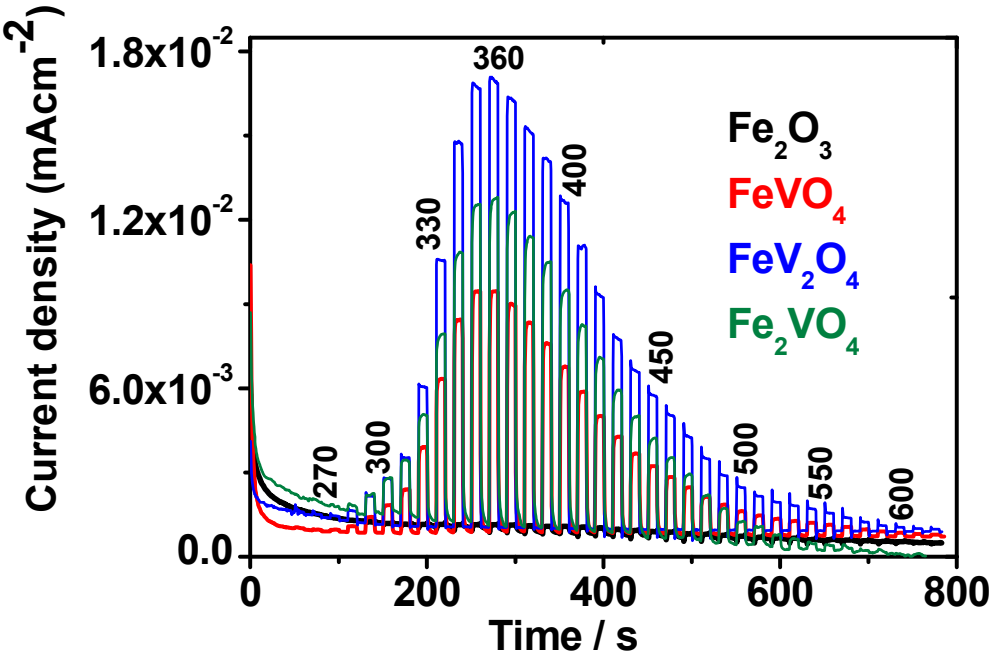

Fig. 9 Photoelectrochemical action spectrum of Fe-V-Oxide semiconductors, calculated from the photocurrent spectra of the material.

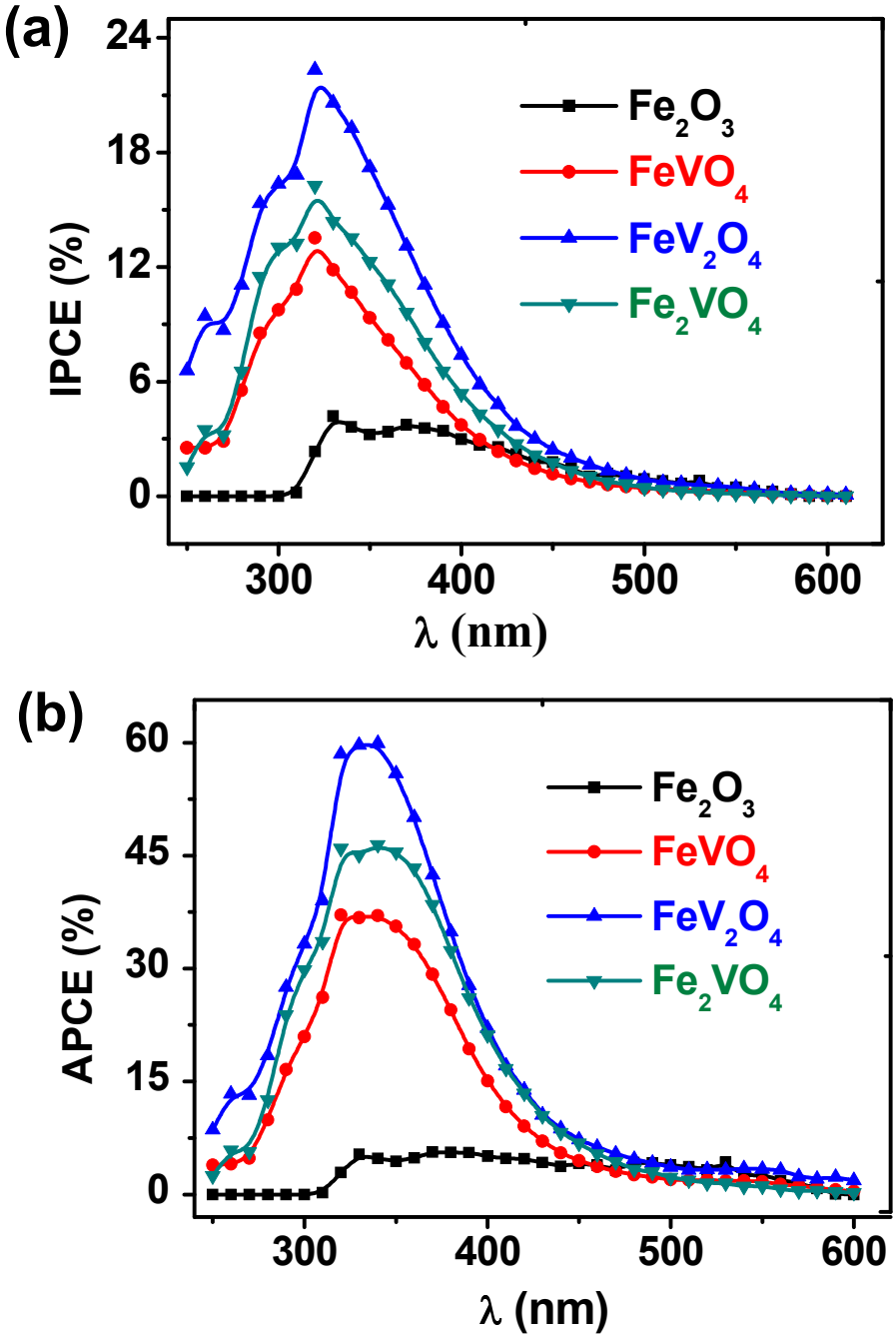

Fig. 10 Variation of **(a) %**IPCE and **(b)** %APCE of Fe-V-oxide semiconductors in 0.1M Na_2SO_4–PBS (pH 7) at applied potential 1.0 V vs. Ag/AgCl reference electrode.

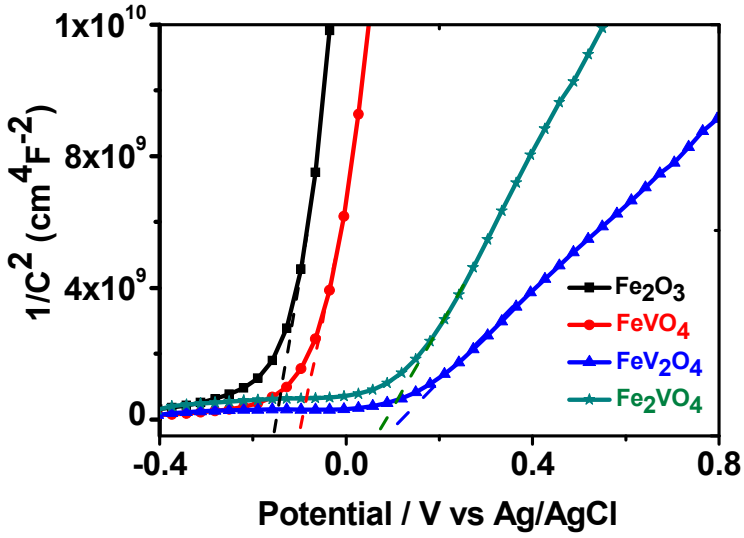

Fig. 11 Capacitance-voltage profile for Fe-V-Oxide compounds recorded at 1000 Hz with an ac amplitude of 10 mV at each potential.

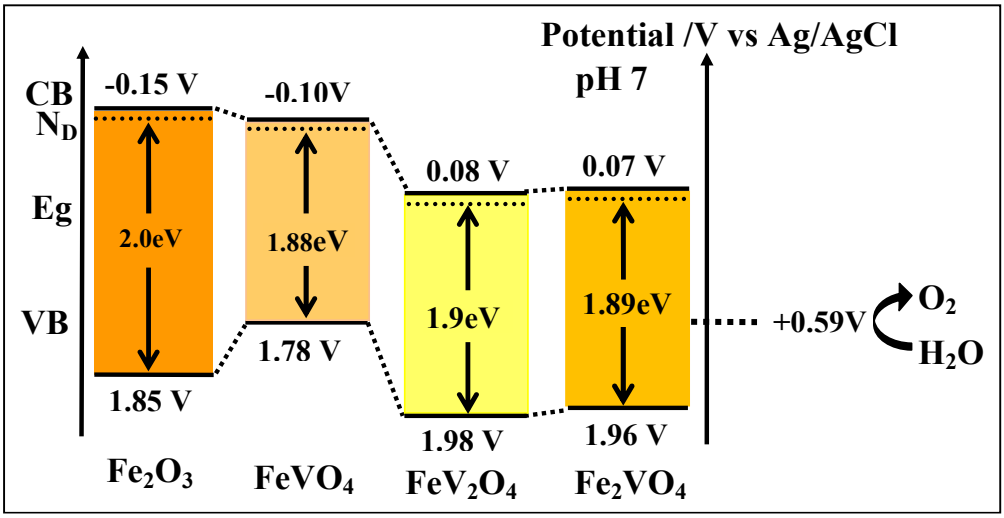

Fig. 12 Schematic band diagrams of Fe-V-Oxides semiconductor-electrolyte interface.

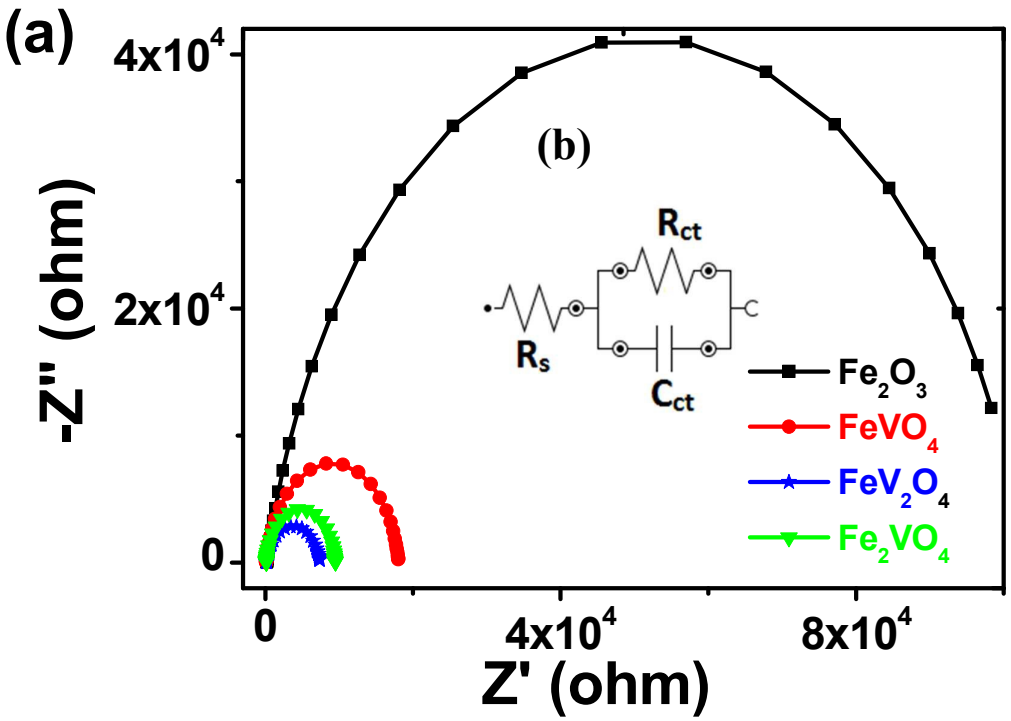

Fig. 13 (a) Nyquist plot of Fe-V-Oxide semiconductors film in 0.1 M Na_2SO_4 with PBS aqueous solutions under UV-Vis light source. (**b, Inset)** Equivalent circuit diagram to analyze the Nyquist plot.

Reference

[1] V. Nivoix, B.Gillot, *Chem. Mater.,* 2000, **12**, 2971-2976.

[2] H. Mandal, S. Shyamal, P. Hajra, B. Samanta, P. Fageria, S. Pande, C. Bhattacharya, Electrochim. Acta, 2014, **141**, 294−301.

[3] K. Sivula, F. L. Formal, M. Gratzel, *Chem. Mater.,* 2009, **21**, 2862–2867.

[4] A.B. Murphy, *Sol. Energy Mater. Sol. Cells,* 2007, **91**,1326 –1337.

[5] S. K. Biswas, J. O. Baeg, *Int. J. Hydrogen Energy,* 2013, **38**, 14451–14457.

[6] A. Dixit, P. Chen, G. Lawes, J. L. Musfeld, *Appl. Phys. Lett.,* 2011, **99**, 141908.

[7] X. Zhou, G. Wu, G. Gao, J. Wang, H. Yang, J. Wu, J. Shen, B. Zhou, Z. Zhang, *J. Phys. Chem. C,* 2012, **116**, 21685−21692.

[8] K. Maeda, K. Domen, *J. Phys. Chem. C,* 2007, **111**, 7851– 7861.

[9] X. Wang, K. R. C. Heier, L. K. Stern, R. Poeppelmeier, *Inorg. Chem.,* 1998, **37**, 6921-6927.

[10] A. Kudo, *Int. J. Hydrogen Energy,* 2006, **31**,197 – 202.

[11]A. Fujishima, K. Honda, *Nature,* 1972, **238**, 37– 38.

[12] O. Khaselev, J. A.Turner, *Science,* 1998, **280**, 425 – 427.

[13] S. Shyamal, P. Hajra, H. Mandal, J. K. Singh, A. K. Satpati, S. Pande, C. Bhattacharya, *ACS Appl. Mater. Interfaces*, 2015, **7**, 18344 –18352.

[14] L. Vayssieres, N. Beermann, S.E. Lindquist, A. Hagfeldt, *Chem. Mater.,* 2001, **13**, 233 –235.

[15] X. Wang, D. A. V. Griend, C. L. Stern, K. R. Poeppelmeier, *Inorg. Chem.,* (2000), **39**,136 –140.

[16] C. Bhattacharya, H. C. Lee, A. J. Bard, *J. Phys. Chem. C,* 2013, **117**, 9633−9640.

[17]H. Xu, H. Li, L. Xu, C. Wu, G. Sun, Y. Xu, J. Chu, *Ind. Eng. Chem. Res.,* 2009, **48**, 10771–10778.

[18] X. Zhang, H. Li, S. Wang, F. F. Fan, A. J. Bard, *J. Phys. Chem. C,* 2014, **118**, 16842–16850.

[19] J. S. Jang, J. Lee, H. Ye, F. F. Fan, A. J. Bard, *J. Phys. Chem. C,* 2009, **113**, 6719–6724.

[20] K. G. Schrantz, S. Tymen, F. Boudoire, R. Toth, D. K. Bora, W. Calvet, M. Gratzel, E.Constable, A. Braun, *Phys. Chem. Chem. Phys.,* 2013, **15**, 1443–1451.

[21] Y. Lin, S. Zhou, S.W. Sheehan, D. Wang, *J. Am. Chem. Soc.*, 2011, **133**, 2398–2401.

[22] C. D. Morton, I. J. Slipper, M. J. K. Thomas, B. D. Alexander, *J Photochem. Photobiol. A,* 2010, **216**, 209–214.

[23] M. A. Mahadik, P. S. Shinde, M. Cho, J. S. Jang, *J. Mater. Chem. A*, 2015, **3** , 23597 – 23606.

[24] J. W. Tang, Z. G. Zou and J. H. Ye, *J. Phys. Chem. B*, 2003, **107**, 14265–14269.

[25] J. Zhan, X. Yang, D. Wang, S. Li, Y. Xie, Y. Xia and Y. T. Qian, *Adv. Mater.*, 2000, **12**, 1348–1351.

[26] K. Fujihara, S. Izumi, T. Ohno and M. Matsumura, J. Photochem. Photobiol., A, 2000, **132**, 99–104.

[27] P. Hazra, A. Jana, M. Hazra, J. Datta, *RSC Adv.*, 2014, **4**, 33662–33671.

[28] S. S. Kulkarni, C. D. Lokhande, *Mater. Chem. and Phys.*, 2003, **82**, 151–156.

[29] L. Zhao, M. P.Y. Wu, K. W. Yeh, M. K. Wu, *J. Solid State Chem.*, 2011, **151**, 1728–1732.

[30] H. Takei, T. Suzuki, T. Katsufuji, *Appl. Phys. Lett.,* 2007, **91**, 072506.

Table of Content: